Aspects of simulating the dynamic compaction of a granular ceramic

2009 Modelling Simul. Mater. Sci. Eng. 17 045003

(http://iopscience.iop.org/0965-0393/17/4/045003)

Modelling Simul. Mater. Sci. Eng. **17** (2009) 045003 (22pp) doi:10.1088/0965-0393/17/4/045003

Aspects of simulating the dynamic compaction of a granular ceramic

John P Borg[1] **and Tracy J Vogler**[2]

[1] Department of Mechanical Engineering, Marquette University, 1515 W. Wisconsin Ave, Milwaukee, WI 53233, USA
[2] Sandia National Laboratories, CA, USA

Received 22 October 2008, in final form 23 October 2008
Published 24 April 2009
Online at stacks.iop.org/MSMSE/17/045003

Abstract

Mesoscale hydrodynamic calculations have been conducted in order to gain further insight into the dynamic compaction characteristics of granular ceramics. With a mesoscale approach each individual grain, as well as the porosity, is modeled explicitly; the bulk behavior of the porous material can be resolved as a result. From these calculations bulk material characteristics such as shock speed, stress and density have been obtained and compared with experimental results. A parametric study has been conducted in order to explore the variation and sensitivity of the computationally derived dynamic response characteristics to micro-scale material properties such as Poisson's ratio, dynamic yield and tensile failure strength; macro-scale parameters such as volume fraction, particle morphology and size distribution were explored as well. The results indicate that the baseline bulk Hugoniot response under-predicts the experimentally measured response. These results are sensitive to the volume fraction, dynamic yield strength and particle arrangement, somewhat sensitive to failure strength and insensitive to the micro-scale Hugoniot and grain morphology. A discussion as to the shortcomings in the mesoscale modeling technique, as well as future considerations, is included.

(Some figures in this article are in colour only in the electronic version)

1. Introduction

The rapid compaction of granular materials is of great interest when developing a better understanding of a variety of processes including those which occur in powder metallurgy, geo-physical flows, ignition mechanisms in energetic materials and meteor impact and crater formation. In order to better understand high strain rate processes in granular materials numeric simulations can provide information that cannot be obtained, or is not cost effective to obtain, from experimentation alone, such as grain on–on grain interactions or large scale parametric studies. Usually, a granular material is modeled as a continuum (i.e. the grains and porosity are treated as a new single material) and is assigned average properties. In

so doing the heterogeneous nature of the material and the grain interactions are lost. In these continuum approaches additional constitutive relations such as the sphere collapse models [1], snowplow [2], P–α [3] or P–λ [4] models are used to govern the removal of porosity. With the continued development of massive computer architectures and parallel programming techniques, computational capabilities have improved such that large domain size and high-resolution simulations are feasible. The result is that simulations that resolve each grain during compaction of a representative sample of the bulk material are possible. The simulations presented here utilize such a high-resolution massively parallel approach within an Eulerian finite volume code known as CTH [5]. Each grain is assigned the properties of the fully dense material, and the macro-scale compaction behavior, including the removal of porosity, is computationally resolved without the use of additional constitutive laws for compaction. This approach is often referred to as a mesoscale (or middle scale) calculation because the intermediate micro- and macro-scales, those associated with the grain dynamics and the removal of porosity, are resolved. Due to the numeric formulation utilized within CTH, however, realistic fracture, material interface tracking and grain on grain contact dynamics are not strictly resolved. More details of the mesoscale simulations will be given in section 2.

A variety of researchers have conducted numeric simulations utilizing a mesoscale approach. These studies ranged in complexity from resolving the shock and compaction interaction of tens to hundreds of grains in a two-dimensional configuration to resolving thousands of mixed material grains in a three-dimensional configuration. Previous researchers have used various computational techniques such as Eulerian hydrocodes, finite-element or discrete-element methods, to resolve the dynamics of a variety of heterogeneous and/or granular materials, including elemental metals and alloys [6–18], earth materials [19], energetic materials [20–33] and ceramic alloys [18, 34–36]. These studies have demonstrated that mesoscale simulations can be used to successfully describe the compaction dynamics without the use of additional constitutive relations, thus corroborating predictions from various analytic porous collapse models and experimental observations [16, 17, 37]. In most of these studies the focus was to numerically predict the bulk material behavior, i.e. Hugoniot behavior. In some cases, simple formulations and simple descriptions on a grain level can combine to resolve complicated dynamics on the bulk scale such as the formation of dynamic force chains, void collapse and hot spot formation.

The work presented here is a follow-on to one such study where the baseline bulk Hugoniot response of granular tungsten carbide (WC) was established using two-dimensional mesoscale simulations [34, 36]. The current study was undertaken over a larger range of driver plate velocities (i.e. particle velocities), from near rigid (soliton) particle behavior to plastic behavior that results in complete removal of porosity of the grain bed. One great potential for mesoscale simulations, which remains relatively unexplored, is investigating the bulk system response by varying many aspects of the mesoscale simulation. In so doing, the mesoscale system can be probed in order to better understand the most dominate physical mechanisms affecting the bulk material response. Thus, the goal of the current study is to further investigate the bulk response of granular WC as a function of varying the micro-material properties, the macro-material description and various computational parameters. The micro-scale properties under investigation here include the description of the grain response (i.e. the zero stress bulk sound speed and Hugoniot slope), Poisson's ratio, dynamic yield and tensile failure strength, while the macro-scale descriptions of interest include bulk material volume fraction, grain morphology, size distribution and arrangement. The results are compared with those obtained in previous mesoscale simulations as well as experimental data [34, 36, 39]

Using mesoscale simulations to investigate the effect of varying micro-scale mechanical properties on the bulk response of heterogeneous systems has been investigated by several

researchers. Conley and Benson performed simulations for pre-compressed granular HMX at stress levels below complete compaction and demonstrated the micro-scale yield stress has a significant effect on the predicted averaged wave speed [20]. They found that increasing the yield strength increases the shock compaction velocity and bulk stiffness. Similar mesoscale simulations by Menikoff demonstrated the same monotonic relationship with respect to strength [25]. As stress levels increase the material undergoes more elastic deformation before flow commences and more elastic energy is stored in each particle. Therefore, the wave speed increases towards the elastic wave limit as the yield stress increases relative to the shock amplitude. At high stress levels, above yield, Benson reported that the average pressure behind the shock front of granular stainless steel was insensitive to micro-scale material strength which was varied from zero to an order of magnitude above the baseline strength [16]. At extremely high stress levels, by varying the dynamic yield strength, mesoscale simulations have been used to tune/estimate the effects of flow viscosity on the bulk behavior of porous HMX [20].

Grain level finite-element analysis has been used to explore the micro-scale tensile stress distribution on brittle ceramic grains (SiC) as a result of static compressive loads [18]. When an arrangement of grains was subjected to a 10 GPa compressive static load, significant regions of tensile stress were established within individual grains that varied from 0 to 6 GPa. This, along with sufficient activation flaws, can lead to significant tensile failure within the compacted grain structure. Investigating how variations in failure strength affects the dynamic compaction of WC within a hydrocode formulation is one of the objectives of this work.

Experimentation to assess the effect of macro-scale bulk parameters including grain size distribution, morphology and sample thickness on the bulk behavior of dynamically compacted heterogeneous systems have yielded a variety of results. Addiss *et al* reported that drop-weight tests on PTFT/Al/W mixtures with a bulk density of 5.9 g cm^{-3} demonstrate higher strength (55 MPa) with fine W particles ($<1\,\mu$m at 14.3% porosity) than denser samples (7.1 g cm^{-3}) which demonstrate lower strength (32 MPa) with coarse W particles ($<44\,\mu$m at 1.6% porosity) [38]. Split Hopkinson bar experiments and subsequent analysis on two different granular porous HMX mixtures: a pre-compacted course grain with a mean diameter (mean diameter of 40 μm) porous HMX and a fine grain (mean diameter 5 μm) porous HMX, indicated that compaction waves travel faster through the fine particulate bed [29, 40] Recent gas gun experiments, which collected temporally and spatially resolved particle velocity records for granular pressed sugar samples with different initial particle size distributions (212–300 or 106–150 μm), reported exceedingly complex behavior in the transmitted wave profiles [33]. Significant differences in low-velocity precursor time of arrival, duration and amplitude, dispersive ramp behavior and variations in the superimposed velocity fluctuations were observed as a function of particle size, sample thickness and impact velocity. However, despite these differences compaction wave speeds were fairly insensitive to variations in grain size distributions. Similarly, point VISAR measurements of granular tungsten carbide did not exhibit variations in wave speed as a function of sample thickness [39].

Herbold *et al* used mesoscale simulations to investigate the possibility that smaller grains self-assemble to form force chains which provide additional strength by creating an underlying material meso-structure that effectively stiffens the bulk system [12]. They theorized that smaller grains are better able to self-assemble to form fully percolated force chains. This is accomplished by force chains being created, destroyed and reassembled (with different particles) in the course of sample deformation aided by material damage and crack formation. However, Benson *et al* reported that the macro-scale response of granular Ni-based alloy and stainless steel systems do not depend on the particle size [16]. They hypothesize that no improvement in bulk strength was observed as a result of their use of strain rate insensitive constitutive models which results in an independence of plastic work as the grain and pore size

varies. Although their conclusions differ from the mesoscale simulations of Herbot *et al*, their simulations did not impose fully percolated grain structures. This suggests that not only grain size but also grain arrangement and possibly morphology within the heterogeneous system can have a combined effect on the bulk response of the system. Using an Eularian hydrocode formulation Benson investigated the effects of morphology on the temperature distribution within a copper powder by numerically simulating the shock compaction of circular and square grain sytems [6]. Although meso-structural variations in stress bridging and temperature were observed as a result of morphology variations, the shock velocity versus particle velocity Hugoniot was invariant to particle morphology.

Towards building an understanding of how meso-structure affects the bulk response of heterogeneous systems, researchers have taken different approaches when representing the macro-scale grain assemblies. In some instances the material realization is imported directly from digitized images of the sectioned material [26, 28, 32]. A more common approach has been to simulate the meso-structure, especially in porous granular systems where a representation of the internal geometry is more difficult to obtain experimentally. The bulk material is then represented by an assembly of simple two-dimensional grain shapes such as circles or rectangles. Benson investigated several different grain packing strategies in order to achieve the required density [6, 14]. He concluded that grain realizations with abnormally large voids result in excessive plastic deformation and jetting. The imposed force chains in Herbold *et al* resulted in increasing the bulk strength of the grain system. Although the effect of meso-structure has been discussed in various mesoscale studies, the effect has not been systematically reported. This study will explore the effect of not only varying grain morphology, circles versus squares or triangles, but will also explore the effect of grain arrangement, i.e. disorder versus ordered crystalline packing.

2. Model setup

The dynamic compaction characteristics of porous granular single crystalline WC powder (manufactured by Kennametal), with a characteristic grain length of 32 μm, have been experimentally investigated using one-dimensional flyer plate experiments [39]. Figure 1(*a*) presents an SEM image of the granular material of interest. The bulk material had an initial volume fraction, ρ_{00}/ρ_0, of approximately 55% and an initial density, ρ_{00}, of 8.56 g cm^{-3}. The numeric experiments were performed using a two-dimensional planar configuration [34]. Figure 1(*b*) presents a schematic of the portion of the experimental test fixture modeled in the simulations presented here, including the rigid driver plate, 2 mm of granular WC, a 1 mm buffer plate and VISAR window. In order to simplify the computations, the impactor was not included in the simulations. Instead the cover plate was modeled as a rigid boundary with a specified velocity, similar to the boundary conditions utilized by others [15]. The calculations were performed for a geometry representing a thin slice of the experiment; a 1 mm (y-direction) $\times$ 2 mm (x-direction) cavity was filled with approximately 1400 particles.

In order to construct a particle distribution which is representative of pouring grains into a test fixture, a numeric procedure for filling the computational domain, with periodic boundary conditions, was implemented [18]. This process initially creates an ordered material distribution with a volume fraction near 80%. In order to achieve the 55% volume fractions of the experiments, particle diameters are reduced while holding the position fixed as suggested by Benson [14]. A portion of the material domain is presented in figure 2(*a*). A grain position randomization technique is used to simulate the disorder associated with pouring. This is accomplished by assigning each particle an initial random velocity and direction. The particles

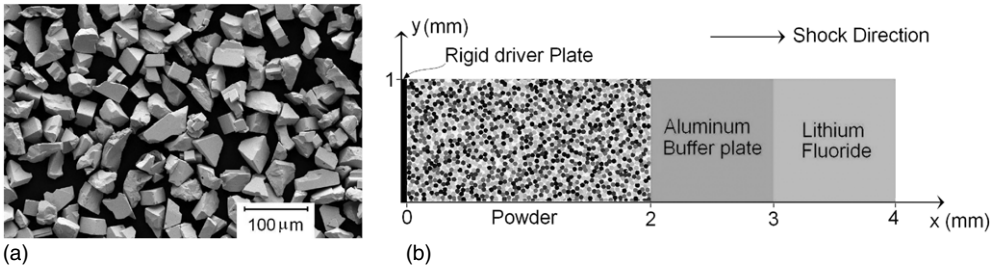

Figure 1. (*a*) SEM image of tungsten carbide (WC) particles used in the experimental study and (*b*) two-dimensional computational geometry showing the computational domain utilized in this work.

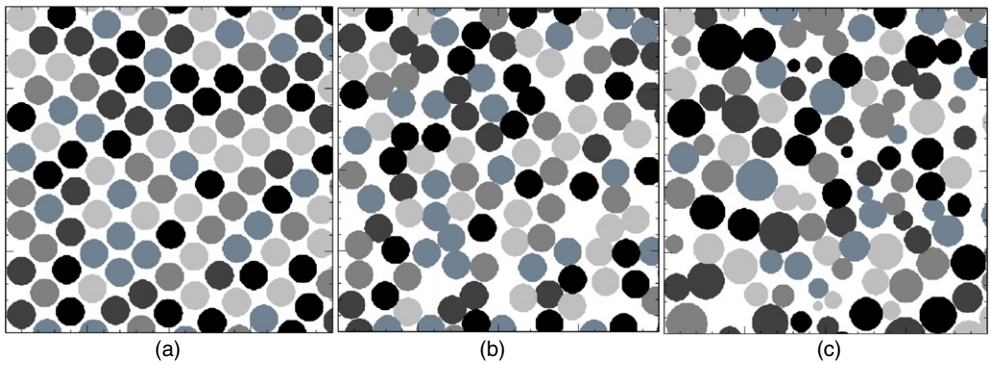

Figure 2. Various initial material distribution of circular particles. (*a*) Particles diameters have been reduced to 32 μm in order to obtain the desired volume fraction (zero standard distribution in diameter), and (*b*) after perturbation. (*c*) Resulting particle distribution with diameter variation (one standard deviation equal to 10 μm). The presented section is 0.16 m^2, 0.4 mm per side and the variations in particles shading is for visualization purposes only.

are then allowed to move in a Brownian-like motion, bouncing off of each other, for an assigned time period equivalent, on average, to that needed to traverse two mean free paths. During this time particle contact is treated as elastic. The resulting particle distribution is presented in figure 2(*b*). The grain size distribution can be specified when the particles diameters are reduced. Unless otherwise stated, the particles size distributions are monodispersed; the results are presented in figure 2(*c*).

Once the material distributions are generated, they are imported as initial conditions into CTH, a massively parallel Eulerian finite volume code. CTH was selected because of its long history in the shock community as well as its successful use in many applications including mesoscale simulations and its ability to handle computationally demanding problems. However, because material interfaces are not resolved it is not completely ideal for this application. In addition, it lacks realistic fracture and grain on grain contact dynamics. The inability to model grain fracture might represent a significant deficiency since fracture may play an important role in the evolution process of shocked ceramics [41]. However, simulations with Eulerian codes which resolve grain level shock interaction have been successfully used to model a variety of material behaviors [11, 24]. (It has been demonstrated that the shock dissipation associated with grain contact and friction is secondary to the visco-plastic work in the absence of large material deformation, as is the case in the simulations presented here [20].)

Table 1. Baseline material and constitutive constants.

Parameter	WC [44–46]	Al[a] [44, 47]	LiF [44, 48]
Density, ρ (g cm^{-3})	15.560	2.703	2.638
Zero stress shock speed, c_0 (km s^{-1})	5.26	5.288	5.15
Hugoniot slope, s	1.15	1.3756	1.35
Grüneisen coefficient, $\Gamma = V(\partial P/\partial E)_V$	1.0	2.14	1.690
Specific heat, C_V (J (g K)$^{-1}$)	0.1723	0.8617	1.9217
Dynamic yield strength, Y (GPa)	5	n/a	0
Poisson's ratio, ν	0.20	0.28	0.50
Fracture strength, σ_s (GPa)	4.0	0.31	∼0.01

[a] Johnson–Cook visco-plastic model [49].

This hypothesis is supported by scanning electron microscopy images of recovered shocked samples [42] and hydrodynamic parametric studies [20].

Unless otherwise stated, the computational resolution was such that a minimum of 12 cells spanned each grain along a single coordinate axis. Periodic boundary conditions were utilized for the top and bottom (y-direction) of the simulation. These calculations required approximately 10 h utilizing 8 nodes (16 processors, 3.06 GHz Intel Xenon processors with 2 GB of RAM) to advance the computational simulation to 4.5 μs.

Material constants utilized for these calculations are listed in table 1. A Mie–Grüneisen equation of state [43] was used for all three materials included in these calculations. The WC, aluminum and LiF equations of state parameters were obtained from the literature [44].

The WC was modeled as linear elastic, perfectly plastic material with values for yield strength and Poisson's ratio obtained from [45]. Experiments have indicated that the spall strength of hot-pressed WC decline rapidly with increased stress [46]; spall strength decreases from a value of 2.06 GPa to 1.38 GPa when shocked to 3.4 Gpa and 7.2 GPa, respectively. The range of shock stress of interest in this investigation varied from 1 to 4 GPa, thus considering the relatively modest shock stress levels of interest here, a constant value of fracture strength of 4 GPa was initially selected. The aluminum (6061-T6) strength was modeled using a rate dependent Johnson–Cook visco-plastic model [49]. The LiF material response was modeled as hydrodynamic, i.e. zero shear modulus. The fracture strength of the aluminum buffer plate was estimated from spall data presented in multiple sources [47, 50]. Given that LiF is assumed to behave as hydrodynamic, i.e. zero shear strength, the fracture strength was also assumed to be small.

3. Results

The following explores the baseline bulk behavior of the dynamically compacted granular WC. The boundary conditions and domain size are varied in order to assess their effect on the bulk response.

3.1. Baseline response

3.1.1. Bulk compaction response. The bulk Hugoniot response of the granular WC was determined using parameters listed in table 1 and the perturbed particle distributions presented in figure 2(*b*). The bulk compaction wave speed or shock speed, U_s, for a prescribed driver plate velocity (i.e. particle velocity, u_p) was obtained using an artificial gauge technique [20]; for more detail on this procedure see [34]. The computational shock velocity versus particle velocity data, U_s versus u_p, over a range of particle velocity from 5 to 600 m s^{-1} is presented

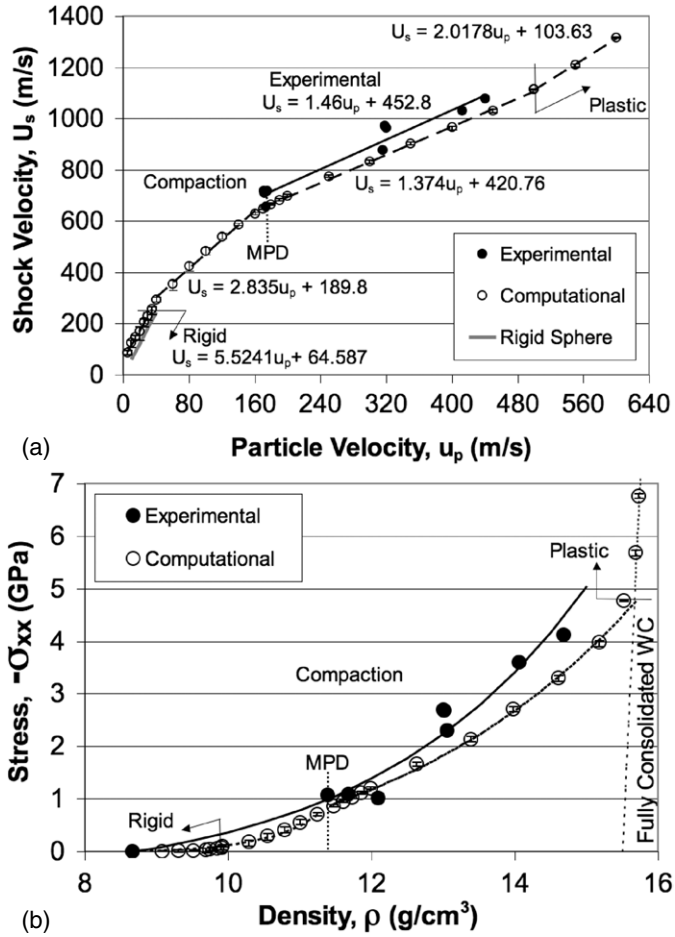

Figure 3. Experimental and baseline computational shock response in (*a*) the shock velocity–particle velocity (U_s–u_p) plane and (*b*) the stress–density plane.

in figure 3(*a*), and represents a significantly larger range of particle velocity than previously investigated [34]. The stress–density plane presented in figure 3(*b*) was obtained by applying the jump conditions to figure 3(*a*). The error bars, which are smaller than the markers in these figures, represent the minimum and maximum compaction wave speed measured within the granular WC. The resulting bulk Hugoniot response presented in figure 3 is referred to hereafter as the baseline response.

In addition to the computational results, experimental data are presented in figure 3 for comparison [39]. The computational results are somewhat less stiff than the experimental results and therefore lie below the experimental Hugoniot. The causes associated with this less stiff response will be explored in greater detail during the parametric study presented later in this paper.

The computational data exhibit several distinct regions of behavior labeled rigid, compaction and plastic; a single linear curve has been fit to the rigid and plastic regions and two linear curves have been fit to the compaction region. As indicated in the figures the rigid and plastic response represents the extreme in behavior whereas the compaction response bridges the two.

At very low particle velocities, below $40\,\mathrm{m\,s^{-1}}$, the response of the material is stiff and dominated by the near rigid behavior of the grains. The increase in density in this region is not obtained by deforming grains but by simply translating the grains and removing porosity. The stiff response results from the fact that grains are not deforming and thus the compaction wave front travels quickly through the grain bed. The rigid region can be described by applying a simple conservation of mass balance to a representative volume, analogous to a one-dimensional bead model [51]. The resulting compaction velocity is $U_\mathrm{s} = u_\mathrm{p}/(1-\rho_{00}/\rho)$; this rigid grain response has been included in figure 3(*a*) and lies along the computationally derived response. The computational response has the same slope as the rigid grain response with a slight increase in the zero stress compaction velocity.

As the driver plate velocity is increased grain deformation begins to play a prominent role in the bulk response of the material. At some particle velocity one would expect the elastic response to dominate the rigid response. To this end, Nesterenko describes a critical particle velocity, u_cr, by equating the rigid grain wave velocity to the velocity of elastic waves propagating through force chains in three-dimensional granular assemblies [52]. The result is a critical particle velocity, u_cr, defined as

$$u_\mathrm{cr} = \left(\frac{16}{25}\right)^{1/5}\left(1-\frac{\rho_{00}}{\rho_1}\right)\left(\frac{2\,(1-2\nu)}{\pi(1-\nu)^2}\right)^{2/5}\left(\frac{34\sigma_\mathrm{s}^{5/2}}{\rho_0^{1/2}E^2}\right)^{4/5} C_\mathrm{L}^{4/5} \tag{1}$$

below which rigid grain behavior dominates and above which elastic force chain behavior dominates. In this expression ν is Poisson's ratio, E is the modulus of elasticity, ρ_1 is the post compaction density which is approximately $9.9\,\mathrm{g\,cm^{-3}}$ from figure 3(*b*) and C_L is the longitudinal sound speed which is $7\,\mathrm{km\,s^{-1}}$ for the WC [45]. From a simple von Mises yield criterion, the shear yield strength σ_s is assumed to be $\sigma_\mathrm{s} = Y/\sqrt{3}$. This together with the values listed in table 1, the critical particle velocity can be calculated using equation (1) to be approximately $89\,\mathrm{m\,s^{-1}}$. As can be seen in figure 3(*a*) the computational results exhibit a change in slope in the U_s–u_p Hugoniot near $40\,\mathrm{m\,s^{-1}}$, which is below this critical particle velocity. This discrepancy will be explored further in section 3.3.2.

As the particle velocity is increased a second change in slope can be observed in the U_s–u_p Hugoniot curve near $170\,\mathrm{m\,s^{-1}}$ or in the stress–density plane at $11.37\,\mathrm{g\,cm^{-3}}$. Utilizing conservation of mass, it can easily be shown that the maximum pack density (MPD) for a two-dimensional planar array of mono-dispersed circular particles (i.e. circular cylinders in three dimensions) is $\rho_\mathrm{MPD} = \pi\rho_0/4$. Using the values listed in table 1, the MPD is therefore $\rho_\mathrm{MPD} = 12.22\,\mathrm{g\,cm^{-3}}$. The MPD is higher than the location of the change in slope in the U_s–u_p Hugoniot near $11.37\,\mathrm{g\,cm^{-3}}$. However, in practice it is reasonable to assume that something less than the theoretical maximum would be achieved by an initially random distribution of particles. Thus the change in slope in the particle–shock velocity curve near $170\,\mathrm{m\,s^{-1}}$ is associated with what is often thought of a rigid locking of the grain particle arrangement. Experimental evidence of slower shock wave velocities at lower particle velocities has been attributed, in part, to longer path length defined by a network of contact points in a three-dimensional arrangement. Researchers speculate that this reduction in wave speed is a result of material motion required to bring adjacent crystals in contact along the various stress bridge paths [33, 53]. This assumption will be discussed in greater detail in the sections that follow. Although rigid locking creates what appears to be a phase transitions, i.e. change in slope in U_s–u_p space, the resulting compaction waves do not exhibit a two wave structure [18].

Finally, as the driver plate velocity nears $500\,\mathrm{m\,s^{-1}}$ the material response stiffens as the behavior transitions to the plastic region. This transition from compaction response to plastic response corresponds to a change in slope in the U_s–u_p plane. The plastic region is defined here as the location where the porous response intersects the fully consolidated WC Hugoniot in

the stress–density plane. The fully consolidated WC Hugoniot, the dashed line in figure 3(*b*), was constructed using the micro-scale parameters for the grain material listed in table 1. The stress at this transition roughly corresponds to the dynamic yield strength specified for the simulations, 5 GPa. At this stress all porosity is removed from the granular material, the theoretical maximum density (TMD) has been achieved, and the response thereafter nearly follows that of the fully consolidated WC Hugoniot in stress–density space. It should be noted that the granular material response in the plastic region does not follow the fully consolidated WC Hugoniot in U_s–u_p space. Table 1 indicates that the zero stress bulk sound speed for fully consolidated WC is over 5000 m s^{-1} whereas the compaction wave speed for the granular WC is always less than 1400 m s^{-1} for the range of driver plate velocities investigated here. The granular material follows a different path to compaction as compared to the path followed by the fully consolidated WC. In the fully consolidated material a stress of 5 GPa could be achieved with a particle velocity of approximately 60 m s^{-1}. The granular material requires much greater energy in order to overcome the moving boundary work (i.e. $\int P\,\mathrm{d}V$) required to achieve equivalent stress and density states. One should not think of plastic states in granular material as ones that lies on the locus of shock states for the initially fully dense material.

3.1.2. Boundary conditions, domain size and resolution study. The lateral, or y-direction, boundary conditions were changed from periodic to either symmetry or outflow boundary conditions in order to assess the effect on the bulk Hugoniot behavior presented in figure 3. The symmetric boundary condition enforces zero velocity at the boundary, i.e. a rigid wall. The resulting bulk response for the symmetric boundary condition differed nearly imperceptibly as compared with the bulk response for the baseline periodic boundary condition. The outflow boundary condition allows mass to flow into ghost cells with zero pressure before being removed from the computational domain; no mass is allowed to enter the mesh. The outflow boundary condition resulted in a softer bulk response with a nearly 5% reduction in the zero stress shock speed, c_0. Since both the periodic and rigid wall boundary conditions satisfy uniaxial strain conditions due to inertial confinement, whereas the outflow boundary condition does not, this variation in bulk response is not unexpected.

Several simulations were performed in which the size of the computational domain was varied in order to assess the effect on the bulk response. The y-direction of the computational domain was increased from the baseline length of 1 mm to as large as 3 mm and the x-direction, i.e. longitudinal direction, was increased from the baseline length of 2 mm to as large as 5 mm. No significant deviation in the dynamic response was observed for any of these variations. These simulated results can be compared to the experimental results that included a target configuration where the longitudinal direction varied from 2 to 5 mm with no measured variation in the compaction wave speed [39].

The mesh resolution was varied in order to assess the effect on the bulk compaction response of the powder. The resolution is described as the number of computational cells across the diameter of a grain, the greater the number of cells the more resolved the grain. For Eularian hydrocode simulations, it has been suggested that 10 cells per grain adequately resolves the grain [54]. Eulerian hydrocode simulations of the dynamic compaction of granular HMX have indicated that the solution is converged for resolutions of 12 cells per grain or higher [25]. The baseline calculation, which contains 12 cells per grain, was repeated with cells per grain varying from 1 to 20; the results are presented in figure 4. The shock velocity is greatly reduced as a result of poor resolution; the smearing of grain boundaries results in a near continuum behavior. As the resolution is increased, so too does the shock velocity. The shock velocity is relatively constant over a range of resolutions from 8 to 15 cells per grain.

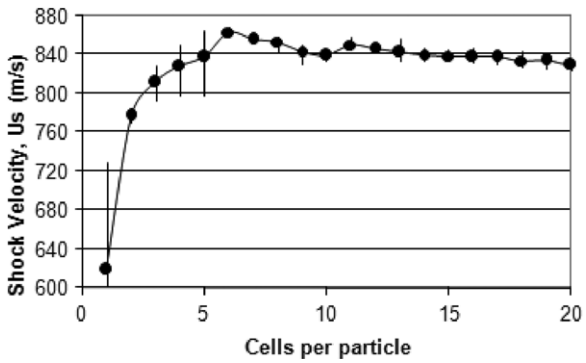

Figure 4. Resolution study illustrating the effect of resolution (number of numeric cells per grain) on shock wave velocity.

3.2. Parametric study: bulk response as a function of micro-scale variations

In order to assess the sensitivity of the bulk response on micro-scale parameters and identify key phenomena associated with the rapid compaction of a porous granular solid, a series of numeric experiments were conducted in which each micro-scale material property listed in table 1 was varied and the resulting bulk Hugoniot response was evaluated. Macro-scale descriptions of the granular solid, such as volume fraction, particle morphology, grain size distribution and material distribution, are investigated in section 3.3.

3.2.1. Micro-scale Hugoniot: slope and zero stress sound speed. A series of calculations were performed where the Mie–Grüneisen model parameters for the grain material, specifically the micro-scale zero stress sound speed, c_0, and Hugoniot slope, s, were varied. The Hugoniot slope for all the grains was increased from 1.15 to 1.42. This increase was motivated by variations reported in the literature. The baseline Hugoniot slope of 1.15 was reported in Steinberg whereas later experiments on Cercom WC, which is a composite consisting of 97.2% WC and 2.8% W_2C by weight, reported the Hugoniot slope to be between 1.309 and 1.419 [45, 46]. Varying the Hugoniot slope did not appreciably change the bulk response through the rigid and compactions regions as compared to the baseline response. The zero stress shock speed, c_0 was varied between 4.93 and 5.63 km s^{-1}. Just as with the Hugoniot slope, the micro-scale zero stress shock speed had little to no effect on the bulk scale response through the rigid and compaction regions. These results imply that the bulk compaction behavior is not sensitive to the underlying material response.

Although the variation of the micro-scale zero stress sound speed, c_0, and Hugoniot slope, s, had little effect on the bulk response through the rigid and compaction regions there was a slight effect on the plastic behavior. Once the porosity is completely removed, the bulk response steepens and follows the fully consolidated Hugoniot. It is in the plastic region that the micro-scale Hugoniot has an effect on the granular bulk behavior. As expected, the now fully consolidated material will follow the fully consolidated Hugoniot as illustrated in figure 3(*b*). Thus if this Hugoniot description is altered, so too is the bulk response in the plastic region. However, given the already stiff behavior of fully consolidated WC and the relatively low stress levels investigated here, the variation in zero stress sound speed, c_0, and Hugoniot slope do not significantly effect the fully consolidated Hugoniot.

3.2.2. Fracture strength. In these hydrocode simulations fracture is not treated as a lattice level phenomena; instead the approach taken here is simplified. The simulations assume that material between cells can support tensile loading until a specified hydrostatic tensile stress is achieved, i.e. the fracture or spall strength. Once this criteria is exceeded failure is enforced by assuming that the yield strength of that material in that specific cell goes to zero. Therefore that material loses all strength, i.e. failed material behaves as an inviscid fluid. In this portion of the parametric study, the micro-scale fracture strength of the WC was varied from near zero to 20 GPa. This two order of magnitude variation from the baseline strength of 4 GPa was motivated by observations that the spall strength of fully consolidated WC rapidly decreases with increased stress [46]; spall strength decreases from a value of 2.06 GPa to 1.38 GPa when shocked to 3.4 GPa and 7.2 GPa, respectively. The motivation to include very low fracture strengths comes from the reported ultimate static tensile strength of WC between 0.3 and 2.0 GPa depending upon the temper [55].

The results of these numeric experiments are presented in figure 5, the arrow indicates the effect of increasing fracture strength. There was little to no change in the bulk response of the granular material as the fracture strength was varied between 2 and 20 GPa. However as the tensile strength is reduced below 2 GPa, the bulk response is also reduced. Below this 2 GPa threshold, grains within the compaction front fail, the local yield stress is reduced and grain bed is more easily compacted. The cumulative effect is a reduction in the stiffness of the bulk material response as the micro-scale fracture strength is reduced. As a result, the change in slope near a particle velocity of 170 m s^{-1}, which is associated with the rigid locking of the grain bed and the maximum packing density, diminishes as the fracture strength is reduced. For a fracture strength of 0.4 GPa there is no change in slope through the compaction region; a single linear fit describes the entire compaction portion of the Hugoniot from rigid to plastic behavior. Given that the CTH hydrocode triggers a reduction in strength as a result of spall, the 'snowplow' [2] behavior for a tensile strength of 0 GPa is understandable.

Since fracture as modeled within the CTH hydrocode is overly simplistic (i.e. the local yield strength, and therefore the ability to sustain compressive load, does not go to zero as a result of fracture), the actual effect on the Hugoniot response as a result of fracture is not known. However two observations can be drawn from these results. First, as the initial compaction wave passes through the grain bed not only is the material compressed but, as a result of the heterogeneous distribution of grains, significant tensile and deviatoric loading conditions are also established. These conditions would not exist as a shock passed through a fully consolidated material. Second, the critical tensile stress levels obtained within the grain bed, 2 GPa, nearly exceed the maximum measured spall strength of 1.38–2.06 GPa. Thus spall, or conditions for tensile fracture, could play a significant role in the compaction of granular solids. This is especially true when one considers multiple wave interactions such as re-shock and release. It is interesting to note that the effect of material failure results in a reduction in strength, which leads to an increase in density with lower required stress. Thus grain failure leads to a softer simulated dynamic response. The experimental Hugoniot is stiffer than the computational Hugoniot and grain failure only exacerbates this discrepancy.

3.2.3. Elastic properties: dynamic yield strength and poisson's ratio. Figure 3 illustrated that the baseline computational response under-predicts the experimental response. In this portion of the investigation the micro-scale dynamic yield strength was varied in order to assess the effect on the bulk Hugoniot response. The yield strength was varied from 2, 5, 7.5, 10, 15 and 25 GPa and the results are presented in figure 6. For the range of yield strengths investigated, an increase in the yield strength increases the bulk response of the granular material and likewise a decrease the yield strength decreases in the bulk response. If the dynamic yield strength is

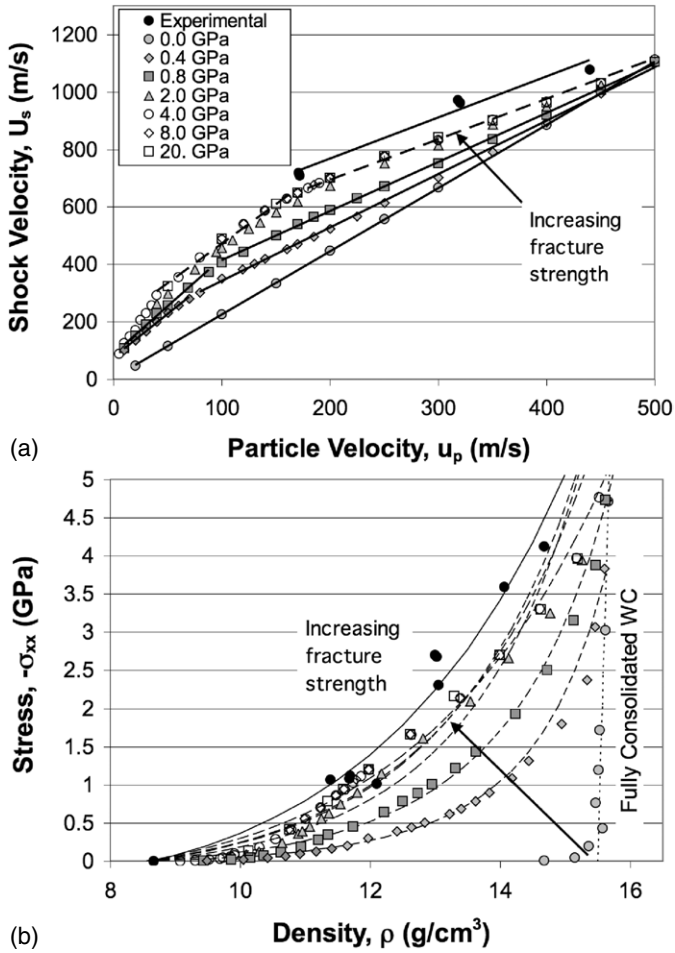

Figure 5. Experimental and computational comparison of (*a*) U_s–u_p plane and (*b*) stress–density plane demonstrating the effect of varying fracture strength. Arrows indicate the effect of increasing fracture strength.

increased from the baseline value of 5 to 7.5 GPa, the computational bulk response closely resembles the experimental bulk response in both the U_s–u_p and stress–density plane.

The U_s–u_p Hugoniot presented in figure 6(*a*) illustrates an interesting feature of the dynamic compaction event: for particle velocities above the rigid grain behavior, approximately 40 m s^{-1}, but below the MPD, approximately 170 m s^{-1}, variations in dynamic yield strength above 5 GPa result in nearly the same bulk behavior. This results from the grains being sufficiently stiff to resist significant yielding while being swept up by the compaction wave. Once the grains rigidly lock at the MPD the bulk behavior exhibits increasing stiffness with increasing yield strength.

The simulated Hugoniot with a dynamic yield strength of 2 GPa intersects the fully consolidated WC Hugoniot at a yield stress of 2.3 GPa and a particle velocity of 300 m s^{-1}. This intersection appears as an increase in slope in U_s–u_p space and the response continues along this line past 600 m s^{-1}. Simulations with higher dynamic yield strength eventually intersect and follow this U_s–u_p Hugoniot when they reach the plastic region.

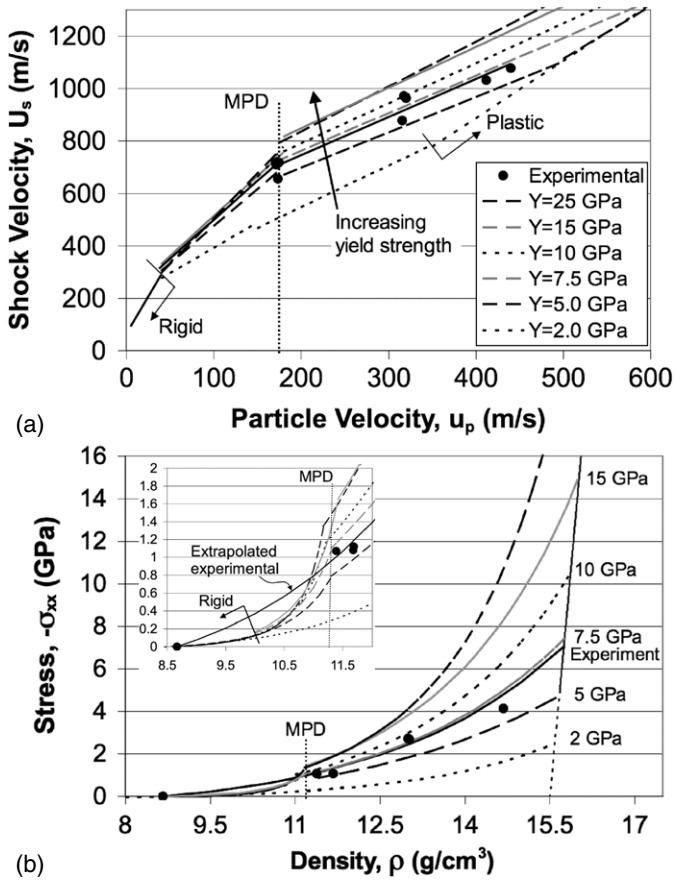

Figure 6. Experimental and computational comparison of Hugoniot demonstrating the effect of increasing the dynamic yield strength. Inset shows low stress region.

As discussed earlier, the complete removal of porosity corresponds to the intersection of the porous granular Hugoniot with the fully consolidated WC Hugoniot; this is presented in figure 6(*b*) for the complete range of yield strengths investigated here. The stress magnitude at this intersection is near, but always greater than, the specified micro-scale dynamic yield strength specified for the simulation. As the yield strength increases the stress required to remove all the porosity increases. The extrapolated fit to the experimental data intersects the fully consolidated Hugoniot at 7.1 GPa, whereas the best fit occurred for the simulated response corresponds to a dynamic yield strength of 7.5 GPa. The inset in figure 6(*b*) illustrates the Hugoniot behavior near the maximum packing density of 11.37 g cm^{-3}; the density at which rigid locking of the grains occurs remains relatively constant regardless of the dynamic yield strength specified for the simulation.

The micro-scale Poisson's ratio, ν, was varied between 0.15 and 0.26; simulations were also performed for Poisson's ratios of 0 and 0.5. Although the baseline value of 0.2 was experimentally determined for Cercom WC, which is a composite consisting of 97.2% WC and 2.8% W_2C by weight, the range under investigation was motivated by various sources which report Poisson's ratio of pure WC to be as high as 0.24 [45, 55]. The resulting bulk dynamic response for values of Poisson's ratio between 0 and 0.26 varied imperceptibly as

compared to the baseline response, and always remained within the error bars presented in figure 3. Increasing Poisson's ratio increases the Hugoniot elastic limit (HEL) with the following relationship, $\sigma_{\mathrm{HEL}} = Y(1-\nu)/(1-2\nu)$. Increasing Poisson's ratio from 0 to 0.26 results in increase in the Hugoniot elastic limit from 5 to 7.71 GPa. Since the average stress in the granular material remains below the dynamic yield stress, variations in HEL had little effect on the bulk dynamic response. A Poisson's ratio of 0.5, i.e. infinitely large HEL and incompressible behavior, resulted in a response curve that snowplowed to the fully consolidated WC Hugoniot.

3.3. Parametric study: bulk response as a function of macro-scale variations

In the previous section, micro-scale parameters listed in table 1 were varied in order to assess their effect on the bulk dynamic response. In this section, several properties associated with the bulk description of the granular material, or macro-scale parameters, will be investigated in a similar fashion. These macro-scale parameters include the initial volume fraction, grain morphology, size distribution and packing order.

3.3.1. Initial volume fraction. In order to assess the effect of initial density on the bulk behavior, the volume fraction, ρ_{00}/ρ_0, was varied from 55% to 78%. This range of variation was selected for two reasons. First, this range of volume fraction is near the MPD of $\rho_{00} = \pi\rho_0/4 = 12.2\,\mathrm{g\,cm^{-3}}$ or 78.5% volume fraction. Second, this range of volume fraction encompasses the range of localized density variations known to exist in some dry granular materials; measurements of density gradients within dry poured Ottawa sand have been reported to be as high as 10% [56].

Figure 7 presents the dynamic response for a range of initial volume fractions; note the same basic structure described above is apparent for each volume fraction investigated, i.e. rigid, compaction and plastic regions. Experimental data for a wide range of porous materials indicate that the zero stress shock speed is a strong function of the initial density while the slope of the U_s–u_p line is largely independent of the initial density [57, 58]. As expected an increase in the volume fraction stiffens the bulk response of the porous medium. Figure 7(*a*) indicates that an increase of the initial volume fraction from 55% to 58.5% increases the granular U_s–u_p Hugoniot response to that of the experiment. However, this same change in initial volume fraction has moderate effect on the bulk Hugoniot response in stress–density space, figure 7(*b*). Although an increase in initial volume fraction can overlay the experimental Hugoniot in one space it is not necessarily true in another Hugoniot space. Further increases in volume fraction continue to translate the U_s–u_p response to faster shock velocities and stiffen the bulk response towards the fully compact Hugoniot in stress–density space.

The dynamic response of a volume fraction realization near the maximum theoretical packing, i.e. 77.9%, exhibits several interesting features in U_s–u_p space not observed in the lower pack densities. The negative Hugoniot slope within the rigid region is a result of sustained elastic waves traversing the grain bed, i.e. stress bridging that extends across the entire grain realization. As described in section 2, the desired volume fractions are achieved by reducing the diameters of the spheres (circles in two dimension) after they have been poured into the initial volume. For near 78% initial volume fraction, the initial geometry results in a close packed arrangement. This close packing sustains fast traveling elastic waves traversing the grain bed. This elastic phenomenon will be investigated in greater detail in future work.

3.3.2. Grain morphology. In order to better understand the variation in the bulk response as a function of grain morphology two additional grain shapes, triangular and square, were

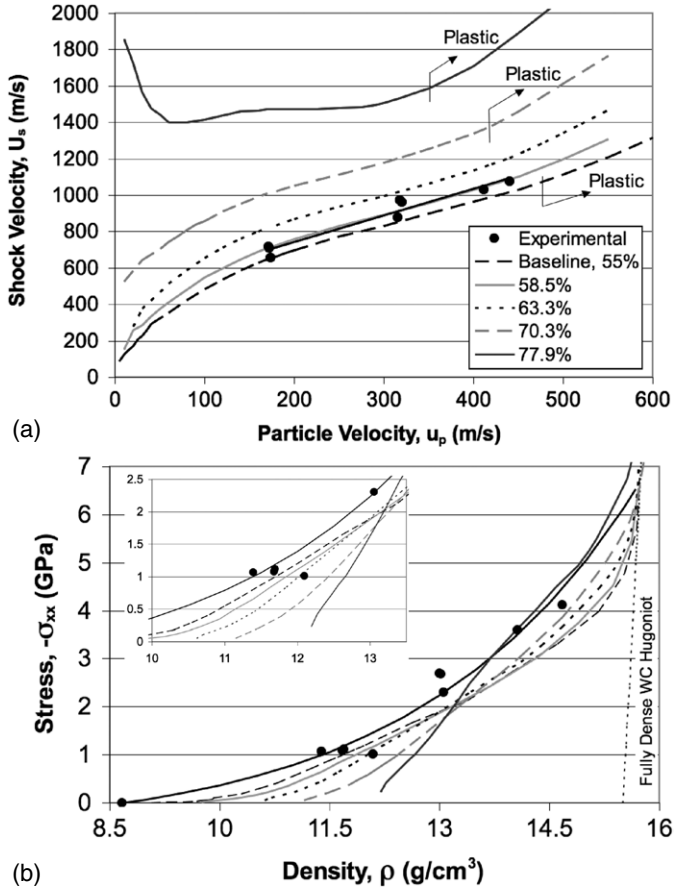

Figure 7. Experimental and computational comparison of Hugoniot demonstrating the effect of increasing the initial volume fraction, ρ_{00}/ρ_0.

explored as compared to circular. A portion of the grain packing illustrating the various grain shapes is presented in figure 8. The methodology for rendering the circular grain realizations is described in section 2. However, given the added difficulty of applying this methodology to square and triangular shaped particles, a different methodology for generating these realizations was utilized. These realizations were generated by replacing each circular grain with either a square or triangular grain with the same characteristic length. While keeping the grain center fixed, each grain was rotated in order to maximize the distance between vertices to the nearest neighbor. The sides of the grains were then increased in small increments until the specified volume fraction was achieved. Thus for each realization the volume fraction was held constant. If while growing a grain's vertex intersected an adjacent grain, i.e. overlap, then both overlapping grains were no longer allowed to increase in size; the effect of this is more pronounced in the triangular realizations presented in figure 8(*c*).

Figure 9 presents the U_s–u_p Hugoniot data as a function of grain morphology. The resulting variations in grain geometry exhibited very little difference in bulk response from the plastic region down into the compaction region. However, as the particle velocity was decreased below the MPD, the more angular the grain the stiffer the response. This is a result of the connectivity of the grain realization and not necessarily a result of morphology. On average

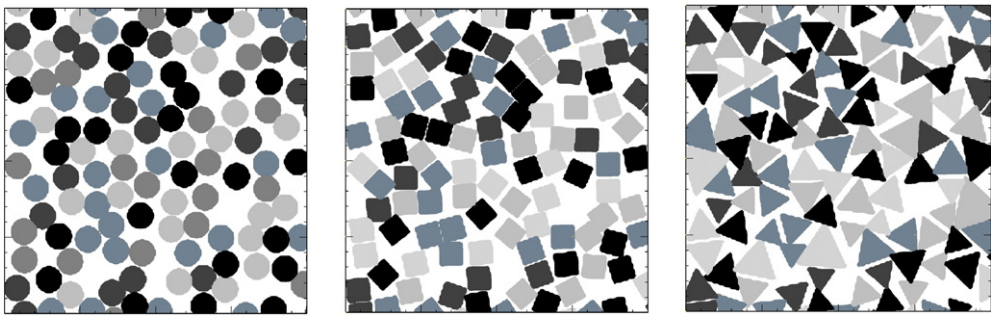

Figure 8. Variations in grain morphology investigated: (*a*) circular, (*b*) square and (*c*) triangular. The section presented is 0.4 mm per side and particle shading is for visualization purposes only.

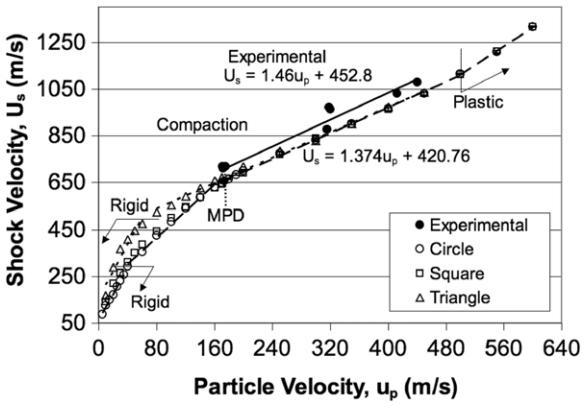

Figure 9. U_s–u_p bulk response as a result of changing grain morphology.

the final characteristic length of the triangular grain was larger than the circular grain. As a result the triangular grain realizations tend to form longer connectivity chains within the grain realizations before compaction. In fact the triangular grain realization is nearly 100% rigidly locked before compaction, each grain touches at least one other grain. This is in contrast to the circular grain realizations where there is void space for grains to freely slide before rigidly locking. This pre-compaction rigid lock within the triangular grain realizations results in longer dynamic force chains, stiffer response below the MPD of $\rho_{\mathrm{MPD}} = \pi\rho_0/4$ and on through the rigid region. The result is a U_s–u_p Hugoniot for the triangular morphology which passes through the MPD without changing slope. The transition from rigid to elastic behavior occurs at a particle velocity of 70 m s^{-1}, better matches the critical particle velocity predicted by equation (1), which for this granular WC was determined to be 89 m s^{-1}. The expression in equation (1) was developed for three-dimensional granular assemblies that have less free space, are closer to rigid lock assemblies, and more similar to the pre-compacted rigidly locked triangular morphology investigated here.

3.3.3. Grain size distribution. In the four sets of simulations, the width of the grain size distribution was increased from a standard deviation of zero, i.e. the mono-dispersed baseline simulation, to a standard deviation of 10 μm. In previous publications we reported that the

grain size distribution had little effect on the bulk Hugoniot behavior. As discussed in section 1, experimental and mesoscale experiments have reported conflicting results as a result of particle size distribution. The results must be viewed in context of the meso-structure, these relevant features include the presence of density variations, the influence of force chains and the bulk realizations, the effect of a binder material, etc. Although the work here supports the assertion that grain size distribution has little effect on the bulk response, when the initial bulk density was carefully controlled and a wider range of grain size distributions were investigated, a slight trend does emerge in the bulk Hugoniot behavior. This trend indicates that as the grain size distribution is increased the bulk Hugoniot response is softened slightly. A monotonic decrease in the Hugoniot response results as the width of the grain size distribution is increased. These results must be juxtaposed against the resolution study presented earlier: as the cells per grain is decreased the Hugoniot response is also decreased. The simulations presented here are for resolutions on the order of 12 cells per grain. Thus small grains would result in low resolutions and reduced strength. This effect could account for the slight softening of the bulk response as the grain size distribution is increased. Conley and Benson acknowledged this effect on their data as well and thus only reported data for a narrow range of particle size [20].

3.3.4. Particle order. In this portion of the investigation the order, or randomness, of the particle arrangement was varied in order to assess the effect on the bulk shock response. When reviewing mesoscale work published in the literature, some researchers include the random motion phase of the arrangement as discussed in section 2 which leads to grain distributions presented in figure 2(*b*), while others omitted it which leads to fairly ordered or crystalline grain arrangements similar to the realization presented in figure 2(*a*) [14, 20, 24, 25]. Even within this body of work where the grains are 'randomly placed', the realizations look more like figures 2(*a*) than (*b*) in that no grain touches an adjacent grain.

A series of numeric experiments were conducted in which the particle perturbation time is varied in order to effectively increase the randomization of the particle distribution. In order to assess the degree of particle order a single randomization metric, μ_{LN}, which is the average of the determinate of the deviatoric terms of the second moment of area tensor. The metric, μ_{LN}, is defined by performing a Voronoi (or Dirichlet) tessellation on the particle distribution that results in discrete area elements, the sum of which is the total area of the domain [59]. The second area moment is calculated for each discrete area and the determinate for the second area moment is calculated for each element. The natural log of the determinant is then taken and fit by a normal distribution (being more normal when transformed); the exponential of the average is then taken to transform it back to the linear coordinates.

Figure 10 presents the randomization metric, μ_{LN}, for the particle realization as a function of perturbation time, i.e. the normalized time particles are allowed to move in a Brownian-like motion. The initial perturbation velocities have been scaled such that 1 unit of time corresponds to the average time it takes for a particle to transit one mean free path. Thus a perturbation time of 3 means that, on average, each particle has undergone three collisions with its nearest neighbor. Figure 10 presents a family of curves each representing particle realizations in which the standard deviation, σ, for the initial size distribution varies from 0 to 10 μm. At a perturbation time of zero, the particles start in a near BCC configuration (see figure 2(*a*)) and are perturbed as time passes; recall the distribution of grains presented in figure 2(*b*) is the same grain distribution presented in figure 2(*a*) perturbed for 4 time units. Thus the randomization metric increases as time increases. Each data point in figure 10 is the average randomization metric, μ_{LN}, from 20 to 30 different realizations, and the error bars correspond to one standard deviation. The upper bound randomization, $\mu_{\mathrm{LN}} = 7.5 \times 10^9\ \mathrm{m}^4$, is found by performing this same procedure using Voronoi points placed completely at random in the domain. The upper

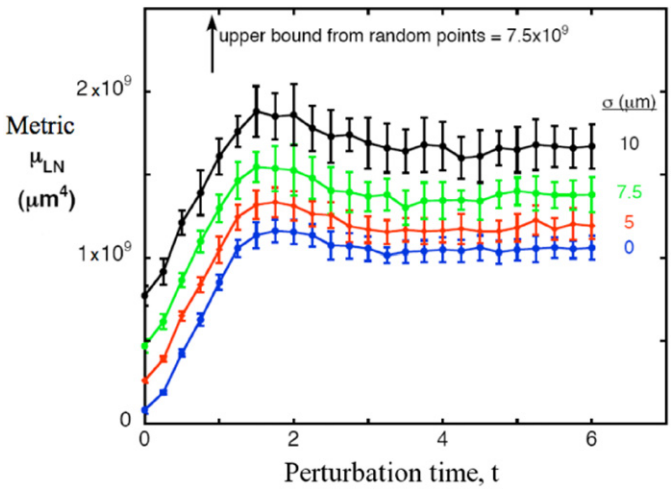

Figure 10. Measure of randomization as a function of perturbation time and particle size distribution. Error bars represent one standard deviation in the randomization metric.

bound cannot be achieved by the particle distributions, of course, because the particles have finite diameters and cannot overlap. For each particle size distribution, i.e. standard deviation, there is a maximum randomization near a perturbation time of 1.6 which roughly corresponds to the average time taken by each particle to touch its nearest neighbor. As time progresses the particles bounce off of each other and randomization metric decays to a steady state value.

In order to assess the effect of particle arrangement on the bulk Hugoniot response two initial geometries were investigated. The first corresponds the crystalline arrangement shown in figure 2(*a*), where the compaction wave is traveling in the [1 1 0] direction or left to right. The second corresponds to this same geometry rotated 45°, in other words the compaction wave is traveling in the [1 0 0] direction. The U_s–u_p bulk Hugoniot response of these two realizations is presented in figure 11; the two crystalline realizations demonstrate anisotropic behavior. Acoustic anisotropy is the rule for all crystal structures, rather than the exception. At high hydrostatic pressures acoustic compression waves travel about 12% faster in the basal plane, i.e. the [1 0 0] direction, of iron than along the [1 1 0] [60]. For the results presented in figure 11, the difference in compaction wave speed is maximized near the MPD where the [1 0 0] wave speed is faster than the [1 1 0] by nearly 55%. This difference in wave speed as a result of crystalline orientation is large enough that the experimentally determined Hugoniot lies within the bounds of the computational results. As the grain arrangement of the crystal structures is perturbed by increasing the perturbation time t, the bulk response of both the [1 0 0] and [1 1 0] arrangements converge to the baseline response presented earlier in figure 3.

For these simulations the area fraction and the grain size distribution was held constant, all that was varied was the grain arrangement as controlled by the amount of time the particles were allowed to interact via Brownian motion. Thus for a given grain size distribution the bulk behavior can be greatly affected depending on how grains are arranged within the computational domain. However, random grain arrangements are most suited to calculations of this type.

4. Discussions and conclusions

This study investigated the dynamic response of granular tungsten carbide utilizing a two-dimensional mesoscale Eulerian hydrodynamic technique as a follow-on to a previous

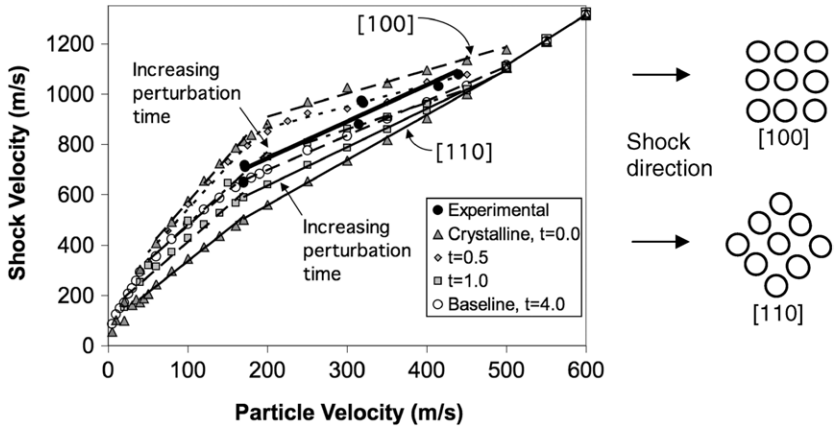

Figure 11. Shock velocity versus particle velocity Hugoniot illustrating the effect of anisotropy associated with initial particle arrangements and perturbation times. Directions correspond to the crystalline orientation as illustrated.

study [34]. The results demonstrate several distinct regions of behavior. Within each region the bulk response can be characterized by a linear U_s–u_p Hugoniot. At low particle velocity the bulk response is dominated by rigid grain behavior. As the particle velocity is increased the response transitions to a mixed elastic–plastic compaction region. The critical particle velocity at which this transition occurs can be estimated by equating the wave velocity from rigid grain behavior to the velocity of elastic waves propagating through force chains. Depending upon the meso-structure and the initial volume fraction, the compaction region can exhibit two regions of bulk behavior. The transition is defined by the maximum packing density. Further increasing the particle velocity results in complete removal of porosity and pure plastic behavior. This third transition can be predicted as the intersection of the granular stress–density Hugoniot with the fully consolidated stress–density Hugoniot. This transition can be estimated where the dynamic yield strength intersects the fully consolidated Hugoniot.

When compared to experimental WC data, the simulated baseline response under-predicts the measured response. A parametric study was conducted to assess the sensitivity of the baseline response to variations in the micro-scale parameters describing each grain. From the parametric study it was found that the bulk response is monotonically sensitive to variations in the micro-scale dynamic yield strength. Increasing or decreasing the yield strength resulted in stiffening or softening the bulk response, respectively. An increase in the yield strength from 5 to 7.5 GPa results in the simulated bulk response matching the experimental response.

Variations of the dynamic failure strength, or spall strength, affected the bulk response only if the micro-scale tensile strength is reduced below 2 GPa. Since the measured spall strength for WC is between 1.38 and 2.06 GPa, the role of spall in the dynamic compaction wave front is still an area under investigation, as is the role of grain failure as successive waves, such as re-shock or release, passing through the powder bed. For this investigation it was found that the micro-scale Hugoniot had little effect on the compaction of porous granular WC. The only measurable effect occurs after the material is completely consolidated: the locus of shock states follows the micro-scale stress–density Hugoniot. Since the compaction response is elastic, Poisson's ratio had little effect too.

As expected the bulk response is sensitive to the initial volume fraction of granular material. Increasing the initial volume fraction stiffens the bulk response. Although the basic behavior of the bulk response is preserved for small variations in volume fraction, for

initially dense grain structures, grain connectivity and elastic wave interactions begin to affect the bulk behavior. The grain arrangement was systematically varied from ordered crystalline to randomized packing. The results indicate that initial grain arrangement can greatly affect the bulk response, especially when compacted to states near the maximum packing density. In addition, simply rotating the crystalline orientation through which the compaction wave passed by 45° has a pronounced effect on the bulk response. These results are significant given the multitude of packing arrangements reported in the literature. Grain morphology affected the bulk response only to the degree to which particle size influences the initial rigidity of the meso-structure. This is in effect prescribing long force chains within the meso-structure. To the degree to which Eularian hydrocode can resolve small grains, particle size distribution had little effect on the bulk response.

Future work will focus on three-dimensional mesoscale simulations. Three-dimensional grain realizations should, in effect, rigidly lock meso-structure and increase the bulk stiffness. The connectivity and longer path lengths should facilitate the transmission of structured waves. In order to better understand the effect of grain contact and micro-scale fracture, a peridynamics mesoscale formulation will be used in concert with Eularian hydrocode simulations.

Acknowledgments

Sandia is a multiprogram laboratory operated by Sandia Corporation, a Lockheed Martin Company, for the United States Department of Energy's National Nuclear Security Administration under contract DE-AC04-94AL85000.

References

[1] Carroll M M and Holt A C 1972 Static and dynamic pore-collapse relations for ductile porous materials *J. Appl. Phys.* **43** 1626–36
[2] Asay J R and Shahinpoor M 1993 *High-pressure Shock Compression of Solids* (Berlin: Springer) p 7
[3] Hermann W 1969 Constitutive equation for the dynamic compaction of ductile porous materials *J. Appl. Phys.* **40** 2490–9
[4] Grady D E and Winfree N A 2001 A computational model for polyurethane foam *Fundamental Issues and Applications of Shock-wave and High-strain-rate Phenomena Proc. EXPLOMET (Albuquerque, NM, USA)* ed K P Staudhammer *et al* pp 485–91
[5] McGlaum J M, Thompson S L and Elrick M G 1990 CTH: a three-dimensional shock wave physics code *Int. J. Impact Eng.* **10** 351–60
[6] Benson D J 1994 An analysis by direct numerical simulation of the effects of particle morphology on the shock compaction of copper powder *Modell. Simul. Mater. Sci. Eng.* **2** 535–50
[7] Williamson R 1990 Parametric studies of dynamic powder consolidation using a particle-level numerical model *J. Appl. Phys.* **68** 1287
[8] Horie Y and Yano K 2002 Non-equilibrium fluctuations in shock compression of polycrystalline α-iron *Shock Compression of Condensed Matter—2001, APS (Atlanta, Georgia)* ed M D Furnish *et al* (MD, USA: AIP) pp 553–6
[9] Case S and Horie Y 2005 Mesoscale modeling of the response of alumina *Shock Compression of Condensed Matter—2005, APS (Baltimore, Maryland)* ed M D Furnish *et al* (MD, USA: AIP) pp 299–302
[10] Nieh T G *et al* 1996 *Acta Mater.* **44** 3781
[11] Bourne N K 2005 Modelling the shock response of polycrystals at the mesoscale *Shock Compression of Condensed Matter—2005, APS (Baltimore, Maryland)* ed M D Furnish *et al* (MD, USA: AIP) pp 307–10
[12] Herbold E B, Cai J, Benson D J and Nesterenko V F 2007 Simulation of particle size effect on dynamic properties and fracture of PTFE–W–Al composites *Shock Compression of Condensed Matter—2007, APS (Kona, Hawaii)* ed M Elert *et al* (MD, USA: AIP) pp 785–8
[13] Yano K and Horie Y 1999 Discrete-element modeling of shock compression of polycrystalline copper *Phys. Rev.* B **59** 13672–80

[14] Benson D J and Nellis W J 1994 Dynamic compaction of copper powder: computation and experiment *Appl. Phys. Lett.* **65** 418–20
[15] Benson D J 1995 The calculation of the shock velocity–particle velocity relationship for a copper powder by direct numerical simulation *Wave Motion* **21** 85–99
[16] Benson D J, Nesterenko V F, Jonsdottir F F and Meyers M A 1997 Quasistatic and dynamic regimes of granular material deformation under impulse loading *J. Mech. Phys. Solids* **45** 1955–99
[17] Nesterenko V F 2001 *Dynamics of Heterogeneous Materials* (Berlin: Springer)
[18] Meyers M A, Benson D J and Olevsky E A 1999 Shock consolidation: microstructurally-based analysis and computational modeling *Acta Mater.* **47** 2089–108
[19] Crawford D A 2005 Using mesoscale modeling to investigate the role of material heterogeneity in geologic and planetary materials *Shock Compression of Condensed Matter—2005, APS (Baltimore, Maryland)* ed M D Furnish *et al* (New York: AIP) pp 1453–7
[20] Conley P A and Benson D J 1999 An estimate of the linear strain rate dependence of octahydro-1,3,5,7-tetranitro-1,3,5,7-tetrazocine *J. Appl. Phys.* **86** 6717–28
[21] Ripley R, Zhang F and Lien F-S 2007 Acceleration and heating of metal particles in condensed explosive detonation *Shock Compression of Condensed Matter—2007, APS (Kona, Hawaii)* ed M Elert *et al* (MD, USA: AIP) pp 409–12
[22] Do I P H and Benson D J 2001 Micromechanical modeling of shock-induced chemical reactions in heterogeneous multi-material powder mixtures *Int. J. Plasticity* **17** 641–68
[23] Baer M R 2002 Modeling heterogeneous energetic materials at the mesoscale *Thermochim. Acta* **384** 351–67
[24] Baer M R and Trott W M 2002 Mesoscale descriptions of shock loaded heterogeneous porous materials *Shock Compression of Condensed Matter—2001, APS (Atlanta, Georgia)* ed M D Furnish *et al* (MD, USA: AIP) pp 713–6
[25] Menikoff R 2001 Compaction wave profiles: simulations of gas gun experiments *J. Appl. Phys.* **90** 1754–60
[26] Eakins D E and Thadhani N N 2007 Mechanistic aspects of shock-induced reactions in Ni + Al powder mixtures *Shock Compression of Condensed Matter—2007, APS (Kona, Hawaii)* ed M Elert *et al* (MD, USA: AIP) pp 1025–8
[27] Milne A M, Bourne N K and Millett J C F 2006 On the un-reacted Hugoniots of three plastic bonded explosives *Shock Compression of Condensed Matter—2005, APS (Baltimore, Maryland)* ed M D Furnish *et al* (MD, USA: AIP) pp 175–8
[28] Benson D J and Conley P 1999 Eulerian finite-element simulations of experimentally acquired HMX microstructures *Modelling Simul. Mater. Sci. Eng.* **7** 333–54
[29] Lowe C A and Greenaway M W 2005 J. Compaction processes in granular beds composed of different particle sizes *J. Appl. Phys.* **98** 123519
[30] Benson D J, Do I and Meyers M A 2001 Computational modeling of shock compression of powders *Shock Compression of Condensed Matter—2001, APS (Atlanta, Georgia)* ed M D Furnish *et al* (MD, USA: AIP) pp 1087–92
[31] Tang Z P and Wang W W 2001 Discrete element modeling for shock processes of heterogeneous materials *Shock Compression of Condensed Matter—2001*, APS (Atlanta, Georgia) ed M D Furnish *et al* (MD, USA: AIP) pp 679–84
[32] Baer M R 2007 Mesoscale modeling of shocks in heterogeneous reactive materials *Shock Wave Science and Technology Reference Library* vol 2, ed Y Horie (New York: Springer)
[33] Trott W M, Baer M R, Castañeda J N, Chhabildas L C and Asay J R 2007 Investigation of the mesoscopic scale response of low-density pressings of granular sugar under impact *J. Appl. Phys.* **101** 024917
[34] Borg J P and Vogler T J 2008 Mesoscale calculations of the dynamic behavior of a granular ceramic *Int. J. Solids Struct.* **45** 1676–96
[35] Benson D J, Tong W and Ravichandran G 1995 Particle-level modeling of dynamic consolidation of Ti–SiC powders *Modell. Simul. Mater. Sci. Eng.* **3** 771–96
[36] Vogler T J and Borg J P 2007 Mesoscale and continuum calculations of wave profiles for shock-loaded granular ceramics *Shock Compression of Condensed Matter—2007, APS (Kona, Hawaii)* ed M Eler *et al* (MD, USA: AIP) pp 773–6
[37] Tong W, Ravichandran F, Christman T and Vreeland T 1995 *Acta Mater.* **43** 230–50
[38] Addiss J, Cai J, Walley S, Proud W and Nesterenko V 2007 High strain and strain-rate behaviour of PTFE/aluminum/tungsten mixtures *Shock Compression of Condensed Matter—2007, APS (Kona, Hawaii)* ed M Elert *et al* (MD, USA: AIP) pp 773–6
[39] Vogler T J, Lee M Y and Grady D E 2007 Static and dynamic compaction of ceramic powders *Int. J. Solids Struct.* **44** 636
[40] Greenaway M W 2005 Measurement of intergranular stress and porosity during dynamic compaction of porous beds of cyclotetramethylene tetranitramine *J. Appl. Phys.* **97** 093521

[41] Meyers M A 1994 *Dynamic Behavior of Materials* (New York: Wiley)
[42] Linse V 1986 *Metallurgical Applications of Shock-Wave and High Strain-Rate Phenomena* (New York: Dekker) pp 29–55
[43] Rice M H, McQueen R G and Walsh J M 1958 Compression of solids by strong shock waves *Solid State Phys.* **6** 1–61
[44] Steinberg D J 1991 Equation of state and strength properties of selected materials *LLNL UCRL-MA*-106439
[45] Dandekar D P and Grady D E 2001 Shock equation of state and dynamic strength of tungsten carbide *Shock Compression of Condensed Matter—2001, APS (Atlanta, Georgia)* ed M V Furnish *et al* (MD, USA: AIP) pp 783–6
[46] Dandekar D P 2004 Spall strength of tungsten carbide *Army Research Laboratory Report* ARL-TR-3335
[47] Moshe E, Eliezer S, Dekel E, Ludmirsky A, Henis Z, Werdiger M and Goldberg I B 1998 An increase of the spall strength in aluminum, copper, and Metglas at strain rates larger than 10^7 s^{-1} *J. Appl. Phys.* **83** 4004–11
[48] Graham R A 1992 *Solids under High-Pressure Shock Compression* (Berlin: Springer)
[49] Johnson G R and Cook W H 1985 Fracture characteristics of three metals subjected to various strains, strain rates, temperatures and pressures *Eng. Fract. Mech.* **21** 31–48
[50] Davison L and Graham R A 1979 Shock Compression of solids *Phys. Rep.* **55** 255–379
[51] Asay J R and Shahinpoor M 1993 *High-Pressure Shock Compression of Solids* (Berlin: Springer) p 12
[52] Nesterenko V F 2001 *Dynamics of Heterogeneous Materials* (New York: Springer) p 89
[53] Sheffield S A, Gustavsen R L and Alcon R R 1997 Porous HMX initiation studies—sugar as an inert simulant *Shock Compression of Condensed Matter—1997, APS (Amherst, Massachusetts)* ed S C Schmidt *et al* (MD, USA: AIP) pp 575–8
[54] Baer M 2006 private communication
[55] Shackelford J F and Alexander W 2000 *Materials Science and Engineering Handbook* (Boca Raton, FL: CRC Press) p 405
[56] Hu C, Ng T T and Altobelli S 2006 Void distributions in samples of Ottawa Sand *Geomechan. Geoeng. Int. J.* **1** 197–206
[57] van Thiel M 1966 *Compendium of Shock Wave Data* Lawrence Radiation Laboratory, University of California, Livermore, CA, UCRL-50108
[58] Marsh S P 1980 *LANL Shock Hugoniot Data* (Berkeley, CA: University of California Press)
[59] Torquato S 2002 *Random Heterogeneous Materials: Microstructure and Macroscopic Properties* (Berlin: Springer)
[60] Jephcoat A and Refson K 2001 Core beliefs *Nature* **413** 27–30